Validation of High Speed Earth Atmospheric Entry Radiative Heating from 9.5 to 15.5 km/s

A. M. Brandis [*][†]

AMA Inc at NASA Ames Research Center, Moffett Field, CA, 94035, USA

C. O. Johnston[‡]

NASA Langley Research Center, Hampton, VA, 23669, USA

B. A. Cruden [§][¶] and D. K. Prabhu [‖][¶]

AMA Inc at NASA Ames Research Center, Moffett Field, CA, 94035, USA

This paper presents an overview of the analysis and measurements of equilibrium radiation obtained in the NASA Ames Research Center's Electric Arc Shock Tube (EAST) facility as a part of recent testing aimed at reaching shock velocities up to 15.5 km/s. The goal of these experiments was to measure the level of radiation encountered during high speed Earth entry conditions, such as would be relevant for an asteroid, inter-planetary or lunar return mission. These experiments provide the first spectrally and spatially resolved data for high speed Earth entry and cover conditions ranging from 9.5 to 15.5 km/s at 13.3 and 26.6 Pa (0.1 and 0.2 Torr). The present analysis endeavors to provide a validation of shock tube radiation measurements and simulations at high speed conditions. A comprehensive comparison between the spectrally resolved absolute equilibrium radiance measured in EAST and the predictive tools, NEQAIR and HARA, is presented. In order to provide a more accurate representation of the agreement between the experimental and simulation results, the integrated value of radiance has been compared across four spectral regions (VUV, UV/Vis, Vis/NIR and IR) as a function of velocity. Results have generally shown excellent agreement between the two codes and EAST data for the Vis through IR spectral regions, however, discrepancies have been identified in the VUV and parts of the UV spectral regions. As a result of the analysis presented in this paper, an updated parametric uncertainty for high speed radiation in air has been evaluated to be [9.0%, -6.3%]. Furthermore, due to the nature of the radiating environment at these high shock speeds, initial calculations aimed at modeling phenomena that become more significant with increasing shock speed have been performed. These phenomena include analyzing the radiating species emitting ahead of the shock and the increased significance of radiative cooling mechanisms.

I.   Introduction

As radiation may contribute a significant fraction of the heat flux for high speed return to Earth trajectories, detailed simulations and experiments have been undertaken to quantify this radiation and evaluate associated uncertainties.[1,2,3,4] Previous studies have identified differences between the experimental measurements taken in the Electric Arc Shock Tube (EAST) facility[5] at the NASA Ames Research Center and theoretical models,[2] such as NEQAIR[6] and HARA.[7,8] Understanding these uncertainties is important for the selection of the thermal protection system (TPS) material, particularly when the radiative heat flux

---

[*]Research Scientist, Aerothermodynamics Branch, Moffett Field, and Member AIAA. aaron.m.brandis@nasa.gov

[†]A significant portion of this work for this article was performed while employed by University Affiliated Research Center, University of California Santa Cruz.

[‡]Research Scientist, Aerothermodynamics Branch , Member AIAA.

[§]Senior Research Scientist, Aerothermodynamics Branch, Moffett Field, and Senior Member AIAA.

[¶]A significant portion of this work for this article was performed while employed by ERC Inc.

[‖]Senior Research Scientist, Aerothermodynamics Branch, Moffett Field, and Associate Fellow AIAA.

American Institute of Aeronautics and Astronautics

becomes large compared to the convective heat flux. Obtaining radiative heating data from flight missions is often difficult, and therefore it is important to measure and validate simulation tools with ground testing facilities. Prior to the high speed EAST measurements presented in this paper, an analysis conducted by Johnston et al.[9] calculated the radiative parametric uncertainty for Earth re-entry to be [32%, -21%] at 15 km/s excluding the effect of ablation products [a]. The present analysis will provide a further insight into the accuracy of theoretical models, and improve understanding of a regime of experimental data that has not previously been validated. The validation will comprise of spectral and spatial comparisons of VUV, UV/Vis, Vis/NIR and IR emission data as measured on the EAST facility with predictive modeling tools.

II.   Description of the EAST Facility

The EAST facility at NASA Ames Research Center was developed to simulate high-enthalpy, "real gas" phenomena encountered by hypersonic vehicles entering planetary atmospheres. Experiments are performed to match flow parameters relevant to flight, such as velocity, static pressure, and atmospheric composition. The basic principle behind testing in the EAST facility is that the shock-heated test gas in the tube simulates conditions behind the bow shock of a re-entry vehicle. EAST has the capability of producing superorbital shock speeds using an electric arc driver with a driven tube diameter of 10.16 cm.[10, 11] The region of valid test gas lies between the shock front and the contact surface that separates the driver and driven gases. The test duration is defined as the axial distance between these two points divided by the local shock velocity. The characteristics of the EAST arc driver result in test durations of approximately 4 - 10 μs. Though short, this test duration is often sufficient to capture the peak non-equilibrium shock radiation and the decay to equilibrium conditions. As the shocked gas arrives at the location of the test section in the tube, spectrometers attached to Charge Coupled Devices (CCDs) are gated and the spectral and spatial emission of the gas are analyzed. EAST utilizes four spectrometers per shot, each associated with four different wavelength ranges. These cameras are referred to as: VUV ($\sim$ 120 – 215 nm), UV/Vis ($\sim$ 190 nm – 500 nm), Vis/NIR ($\sim$ 480 nm – 900 nm), and IR ($\sim$ 700 nm – 1650 nm).

II.A.   Test Conditions

The nominal test conditions were chosen to be representative of the Multi Purpose Crew exploration Vehicle's (MPCV's) re-entry into Earth's atmosphere during a lunar return mission. This corresponds to a shock speed of approximately 10 km/s, free stream pressures ranging from 13.3 Pa (0.1 Torr) to 26.6 Pa (0.2 Torr)[12, 13] and a test gas composition of 79% N_2 and 21% O_2 by mole. However, in order to better ascertain the dependency of the shock speed on radiation, shots were aimed at expanding the testing conditions to encompass speeds up to 15.5 km/s. This expanded data-set provides a more complete picture to analyze the relationship between shock speed and emitted radiation and allows for a more robust comparison with simulations. Figure 1 shows a comparison of EAST testing conditions with various flight missions that re-entered Earth's atmosphere. The flight mission conditions have been scaled to match density by accounting for the difference in ambient temperature in the upper atmosphere versus the laboratory. Four sets of EAST data are shown, denoted Test 46,[10] 47,[5] 50[12, 13] and 52. Data from these tests may be obtained publicly by contacting the authors.

III.   Analysis Approach

III.A.   Brief Description of Codes

Non-EQuilibrium AIr Radiation (NEQAIR) is a line-by-line radiation code which computes spontaneous emission, absorption and stimulated emission due to transitions between various energy states of chemical species along a line-of-sight.[6] Individual electronic transitions are considered for atoms and molecules, with the molecular band systems being resolved for each rotational line. Since the report of Whiting et al.,[6] numerous updates have been incorporated into NEQAIR, such as: using the latest version of the NIST atomic database (version 5.0),[14] using the bound-free cross sections from TOPbase[15] as opposed to inverting the absorption cross-sections of Peach,[16] incorporating the CO_2 database from CDSD-4000,[17] parallelization and improvements to the mechanics of QSS. This latest version of NEQAIR is known as v14.0.[18]

---

[a]This uncertainty bound is the sum of all the parametric uncertainties listed in Johnston et al.[9] except for those related to ablation products.
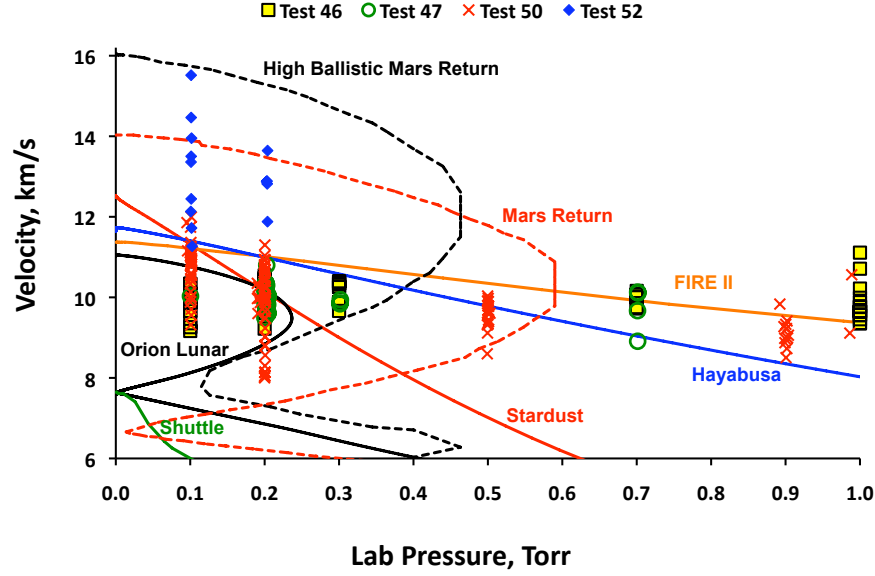
Figure 1. Comparison of EAST testing conditions to various flight missions that re-entered Earth's atmosphere and proposed Mars return missions.

The High-temperature Aerothermodynamic RAdiation (HARA) model applied in the present study is discussed in detail by Johnston et al.[7,8] HARA is based on a set of atomic levels and lines from the NIST[19] and Opacity Project databases.[20] A line-by-line approach is used for atoms and optically thick molecules, while a smeared band model (SRB) is used for optically thin molecules. This approximate molecular model is accurate for the present lunar return applications because the emitting molecular bands are optically-thin.[21] The SRB model has also been shown to be sufficient for modeling strongly absorbing VUV band systems.[7] As with NEQAIR, the atomic bound-free model is composed of cross sections from TOPbase,[15] however, in HARA these cross sections which were curve fit by Johnston.[7]

The process for conducting the simulations is to perform the calculation at a very high spectral resolution followed by a convolution (scan) with a slit function. The slit function used in the simulations is either a square root of a Voigt function or a combination of a Gaussian and a Lorentzian function that has been fit to the measured instrument line shape for the particular settings for each shot.[13]

While NEQAIR and HARA share many common features, in particular using the atomic lines and levels obtained from NIST,[19] there are some important differences between the two codes. These differences being the inclusion of the radiative attachment mechanism and TOPbase atomic lines[7] in HARA, both of which are not implemented in NEQAIR. A summary of the line and band systems for Earth entry implemented in NEQAIR and HARA is shown in Table 1.

III.B. Issues Related to Modeling of EAST Results

The simulations for modeling the radiation measured in the EAST facility are an idealized approximation of the actual tube flow phenomena. Firstly, the simulations are based on an assumption that the flow reaches equilibrium, with the post-shock conditions being calculated by CEA (Chemical Equilibrium with Applications).[22] The reason for using equilibrium post-shock conditions is due to CFD computations for flight showing that the flow relaxes to an equilibrium state approximately 0.4 cm behind the normal shock, as seen in Fig. 2. The nonequilibrium peaks seen in translational temperature and electron number density are at a finer resolution than what is currently measured during the EAST experiments. Figure 2 shows the results of a computation performed on a hemisphere of 1 m radius, with the stagnation line taken as representative of the region of relaxation. A 1 m radius was used in the calculation to provide a shock stand off distance sufficiently large enough to allow the gas directly behind the shock to not be affected by the presence of the hemisphere. A two-dimensional grid of size 160 × 245 (stream-wise × normal) was constructed using GRIDPRO[23] with the grid being large enough to accommodate the bow shock. Flow computations were performed using v4.02.2 of an in-house code, DPLR.[24] An 11-species (N_2, O_2, NO, NO^+, N_2^+, O_2^+, N, O, N^+, O^+, e^-) gas model was used in the computations; the reaction mechanism and rates

American Institute of Aeronautics and Astronautics

Table 1. Line and band systems for radiative heating relevant to Earth entry implemented in NEQAIR and HARA

Species	Systems	NEQAIR	HARA
N, O	NIST lines/multiplets	✓	✓
N, O	TOPbase lines/multiplets		✓
N^+, O^+, e^-	bound-free and free-free continua	✓	✓
N^-, O^-	bound-free and free-free continua		✓
N_2	1st-positive ($B\,^3\Pi_g \to A\,^3\Sigma_u^+$)	✓	✓
	2nd-positive ($C\,^3\Pi_u \to B\,^3\Pi_g$)	✓	✓
	Carroll–Yoshino ($c_4'\Sigma_u^+ \to X^1\Sigma_g^+$)	✓	✓
	Worley-Jenkins ($c_3'\Pi_u \to X^1\Sigma_g^+$)	✓	✓
	Birge-Hopfield I ($b\,^1\Pi_u \to X^1\Sigma_g^+$)	✓	✓
	Birge-Hopfield II ($b'\,^1\Sigma_u^+ \to X^1\Sigma_g^+$)	✓	✓
	Lyman-Birge-Hopfield ($a\,^1\Pi_g \to X^1\Sigma_g^+$)	✓	
	Worley ($o_3\,^1\Pi_u \to X^1\Sigma_g^+$)		✓
O_2	Schumann-Runge ($B\,^3\Sigma_u^- \to X\,^3\Sigma_g^-$)	✓	✓
NO	β ($B\,^2\Pi \to X\,^2\Pi$)	✓	✓
	γ ($A\,^2\Sigma^+ \to X\,^2\Pi$)	✓	✓
	δ ($C\,^2\Pi \to X\,^2\Pi$)	✓	✓
	ϵ ($D\,^2\Sigma^+ \to X\,^2\Pi$)	✓	✓
	β' ($B'\,^2\Delta \to X\,^2\Pi$)	✓	✓
	γ' ($E\,^2\Sigma^+ \to X\,^2\Pi$)	✓	✓
N_2^+	1st-negative ($B\,^2\Sigma_u^+ \to X\,^2\Sigma_g^+$)	✓	✓

associated with this model can be found in the work of Park.[25] In addition to chemical nonequilibrium, the flow field was assumed to be in thermal nonequilibrium as well. Consequently, a two-temperature (T-T_v) model was used. In the two-temperature model employed, the translational, rotational and free-electron modes of molecules are assumed to be in equilibrium (T=T_{trans}=T_{rot} = T_{e^-}), and are distinct from the vibrational and electronic modes of the molecules (T_v =T_{vib}=T_{elec}). The CFD equilibrium state seen in close vicinity behind the shock is in good agreement with the thermodynamic equilibrium state predicted by CEA, as seen in Fig. 2. As the distance to the stagnation point decreases, the electron number density calculated by CFD can be seen to increase when compared to CEA equilibrium. This is currently believed to be an artifact in the kinetics implemented in the CFD, and not representative of a physically accurate phenomena. Therefore, according to the CFD results, the flow region in EAST that is deemed to show steady state radiance should nominally have reached equilibrium.

It is assumed that the stagnation-line flow near the shock is analogous to the flow in the shock tube. However, due to the nature of the shock tube environment, with a decelerating flow, boundary layer growth and limited test time, there is no guarantee that the EAST flow actually reaches thermodynamic equilibrium. It is also possible that the reaction rates used in CFD are not sufficiently well known, particularly when applied to a flow with this level of dissociation and ionization, and therefore may not adequately predict the rate of relaxation to equilibrium. Using this equilibrium assumption in the simulations could lead to discrepancies between the predicted and measured results. Furthermore, the equilibrium calculations presented in this paper are based on the underlying assumption that the inviscid flow is adiabatic (i.e., total enthalpy is conserved across the shock), and therefore do not account for effects such as radiative cooling. Initial calculations attempting to analyze the effect that radiative cooling has on the state of the gas is presented in a following subsection.

III.C. Comparison of Predictions and EAST

This section presents an analysis and comparison of NEQAIR, HARA and EAST data for the VUV, UV/Vis, Vis/NIR and IR spectral regions coinciding with the four spectral ranges of the spectrometer. The relaxation
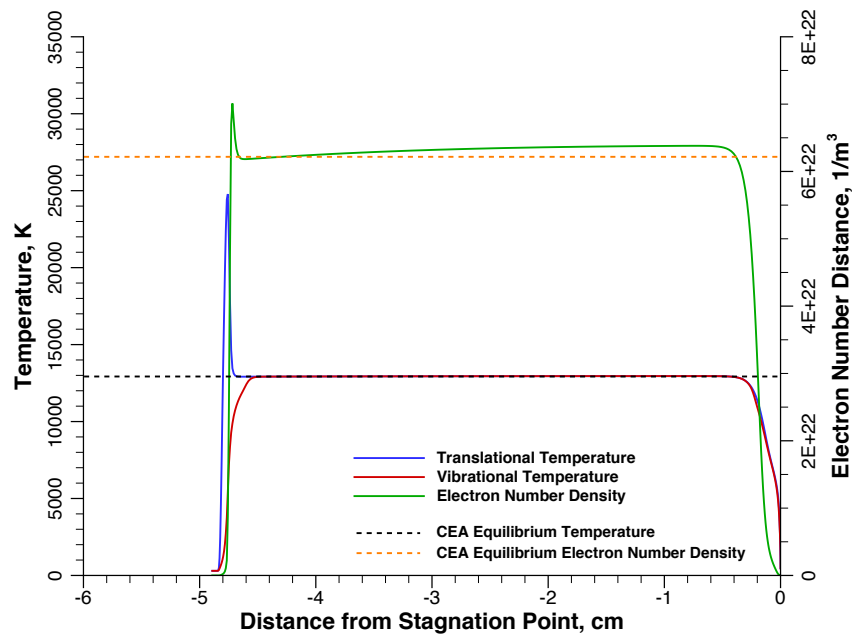
Figure 2. Relaxation of electron number density, translational and vibrational temperature behind a shock at 13 km/s and 0.2 Torr.

of the radiation behind the shock front in EAST is analyzed in order to identify the region of shocked gas that has reached a steady-state of radiance. As mentioned in the previous section, based on the comparison to relaxation length scales found in CFD, this steady region is assumed to be in equilibrium. The comparisons are conducted using the same methodology previously published by Brandis et al.[13] The basic idea being that NEQAIR and HARA are used to simulate the post-shock equilibrium state for all spectral features and regions corresponding to the test conditions performed in EAST. Figures 3 and 4 show a spectral comparison of NEQAIR, HARA and EAST for four spectral regions ranging from the VUV through to the IR at 15.52 km/s and 0.1 Torr, and at 13.64 km/s and 0.2 Torr, respectively. These experiments were chosen as they represent the two fastest shots from the recent EAST testing at both pressures.

The VUV spectral region below 190 nm is a very difficult region in which to obtain data due to the absorption of the emitted radiation by ambient oxygen. Therefore, the collection optics and spectrometer must be located in a vacuum environment, and special windows are required to allow the transmission of photons (UV-Silica for > 165 nm, Sapphire for > 145 nm, and LiF or MgF_2 for > 120 nm). For the current high speed studies, tests were conducted using only the UV-Silica windows to control consumable costs, so data is limited to > 165 nm. The main spectral feature of interest in this range being the nitrogen line at 174 nm. Figures 3(a) and 4(a) show a spectral comparison of NEQAIR, HARA and EAST in the VUV spectral range. The figures show a comparison between 170 and 180 nm with the integrated intensity versus wavelength also presented. Both codes predict the integrated VUV radiation adequately for both conditions, within 20% of the EAST result.

The UV/Vis region of the spectrometer is one of the more challenging regions to simulate, predominantly due to the background continuum radiation being dominant in this region which has been shown to be substantially under-predicted by theoretical models in the past.[26] The analysis of the UV/Vis region of the spectrum is also approached in a different manner to the VUV region due to the superposition of atomic emission lines with dominant background continuum emission. This means that unlike the VUV region, where single spectral features can be analyzed, the UV/Vis spectral region needs to be analyzed as a whole, as it is very difficult to separate the various emitting features. Figures 3(b) and 4(b) show comparisons of NEQAIR, HARA and EAST for the UV/Vis region of the spectrum where the radiance is dominated by the background continuum. Overall, both codes are within 22% of the experiment for both conditions for this spectral range. However, in contrast to previous findings that showed HARA was in better agreement with EAST than NEQAIR for the UV/Vis region (albeit for lower shock speed conditions, < 11 km/s[13]), these figures indicate that for higher shock speeds NEQAIR provides better agreement. Potential reasons for this are discussed later in the paper. This spectral region also shows evidence of TOPBase lines implemented

American Institute of Aeronautics and Astronautics

in HARA which appear to be significantly stronger than the EAST measurements indicate. These lines can be seen between 355 to 375 nm. There are also lines present in both NEQAIR and HARA emitting between approximately 425 to 431 nm, that are not evident in the EAST results.

The Vis/NIR and IR regions of the spectrum are typically easier to simulate due to the radiation being emitted from atomic species only and the influence of the background continuum emission being less significant. Results for these regions are shown in Figs. 3(c), 3(d), 4(c) and 4(d). Figures 3(c) and 4(c) show that for the Vis/NIR region, the integrated values of EAST and both codes agree very well (all within 11%). Figures 4(d) and 4(d) show that for the IR region, the integrated values of EAST and both codes also agree well (all within 14%).

(a)

(b)

(c)

(d)
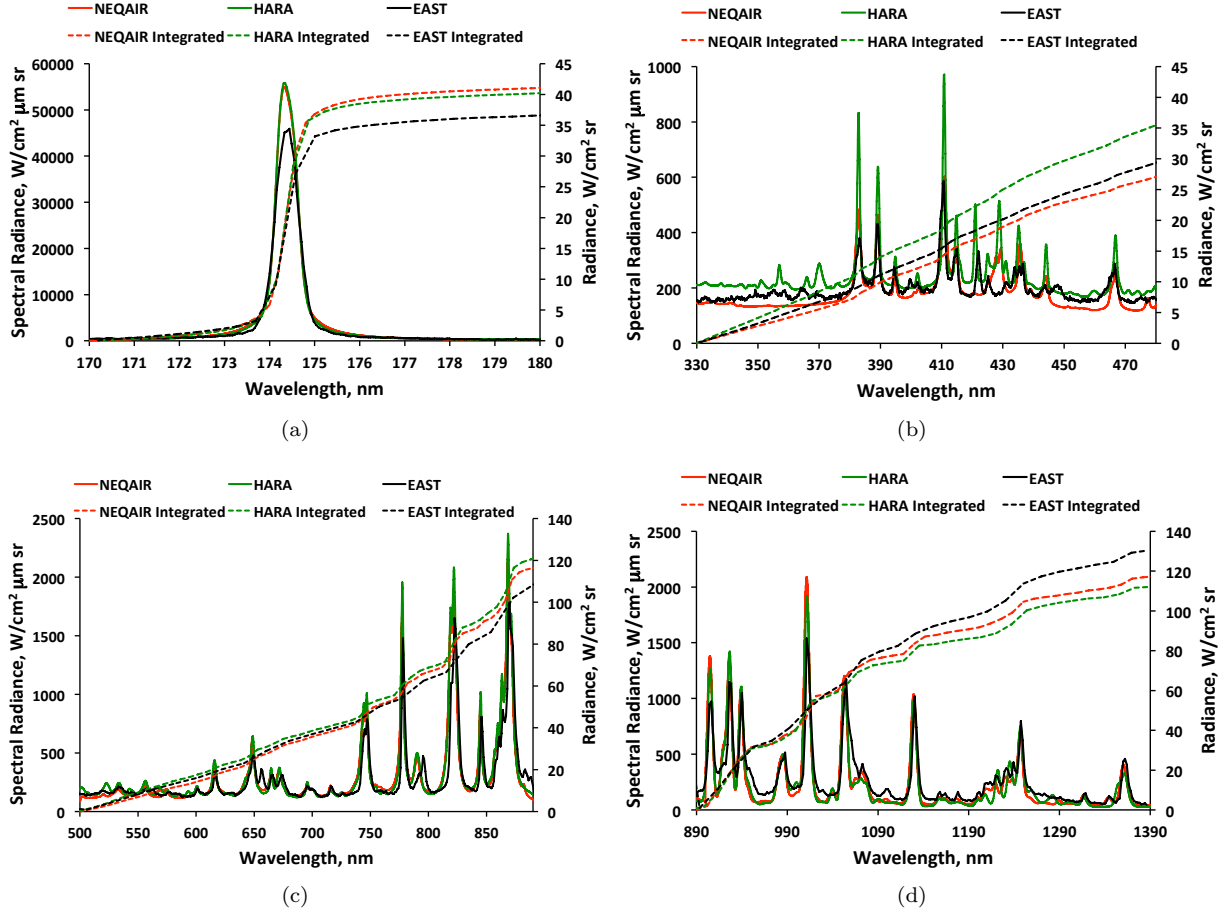
Figure 3. Spectral comparison of NEQAIR, HARA and EAST data at 15.52 km/s and 0.1 Torr for the (a) VUV, (b) UV/Vis, (c) Vis/NIR and (d) IR.
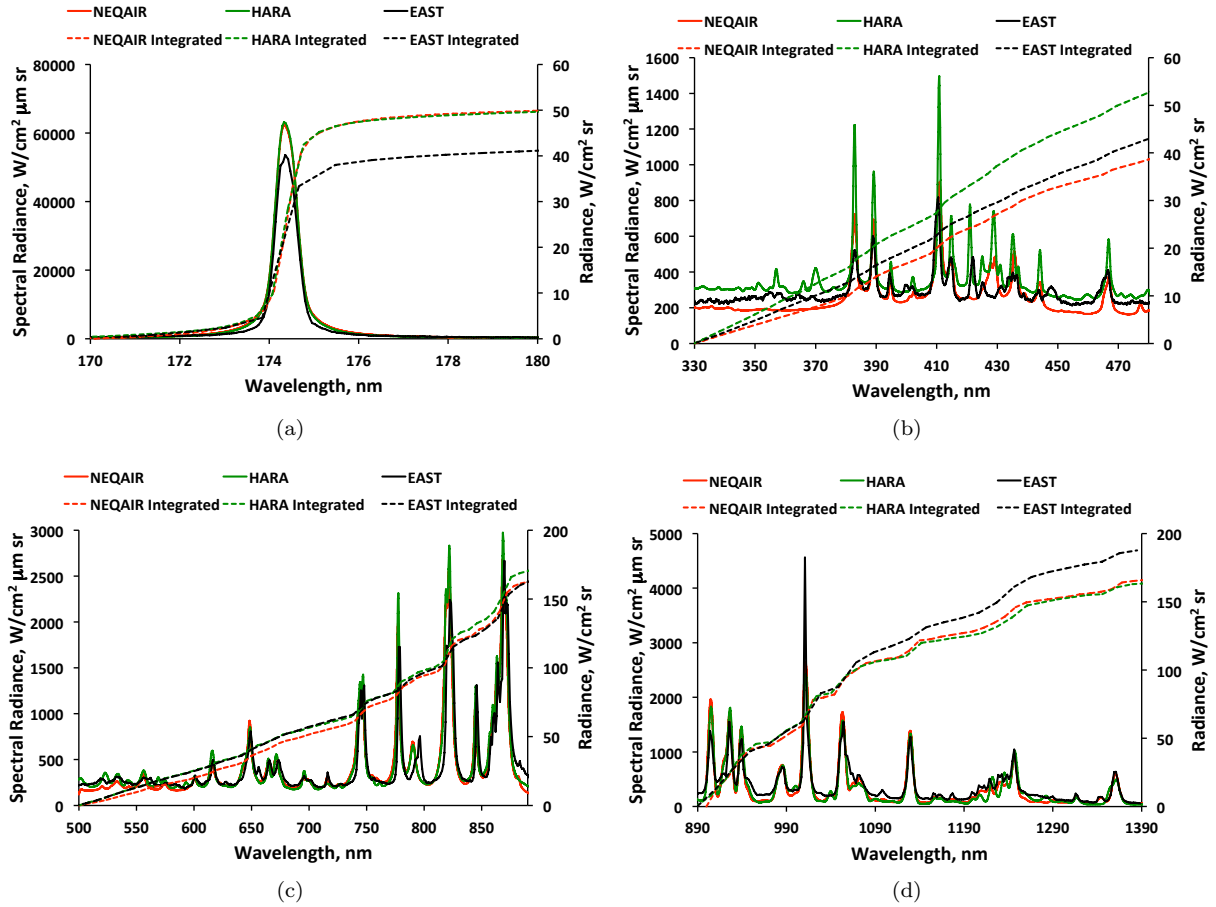
American Institute of Aeronautics and Astronautics

Figure 4. Spectral comparison of NEQAIR, HARA and EAST data at 13.64 km/s and 0.2 Torr for the (a) VUV, (b) UV/Vis, (c) Vis/NIR and (d) IR.

American Institute of Aeronautics and Astronautics

III.D. High Speed Phenomena

Due to the high speeds of the recent shots in EAST, new radiating phenomena have been observed, such as identifiable pre-shock radiation and a significant effect due to radiative cooling. These effects can be demonstrated by showing the integrated radiance for the Vis/NIR spectral region at 15.52 km/s and 0.1 Torr, see Fig. 5(a). The radiance profile versus distance shows several distinct regions. The region from approximately 0 - 2 cm predominately shows radiation that has been smeared ahead of the shock due to the instrument function combined with a small amount of what appears to be pre-cursor radiation, as shown in Fig. 5(b). Figure 5(b) shows the spectral radiance in front of the shock, after correction for camera smearing. The smearing is assumed to be described by a constant scaling of spectral radiance at the shock front. This corrected spectrum is comprised of emission from the N_2 2nd Positive transition which is not observed behind the shock. From 2.6 - 3.5 cm, the nominal equilibrium region can be identified, and following this from 3.5 - 8.5 cm appears to be valid test gas showing the influence of radiative cooling. The influence of radiative cooling has been modeled using the coupled LAURA/HARA code. These simulations have implemented the tangent slab radiation transport assumption, and although this assumption is not appropriate for a shock tube geometry, it should provide an estimate of radiative cooling at the high velocity conditions. A comparison of EAST and LAURA/HARA is presented in Fig. 6(a). The figure shows a comparison with both uncoupled (no radiative cooling) and coupled (with radiative cooling) LAURA/HARA solutions. Figure 6(a) shows that the coupled solution does indeed show a significant effect due to radiative cooling, however, the rate of cooling is under-predicted when compared to the experimental result. This is consistent with theory as using the tangent slab approximation should under-estimate the amount of cooling. This is due to the approximation assuming a large volume of radiating gas, which could provide more absorption to each spatial point. The translation and vibration temperature profiles corresponding to these simulations is presented in Fig. 6(b). This figure shows that the temperature can be up to 5% less for the coupled case in the region just behind the shock. Figure 6(b) also shows that by including radiative cooling, the shock stand off distance is reduced by approximately 6 cm.
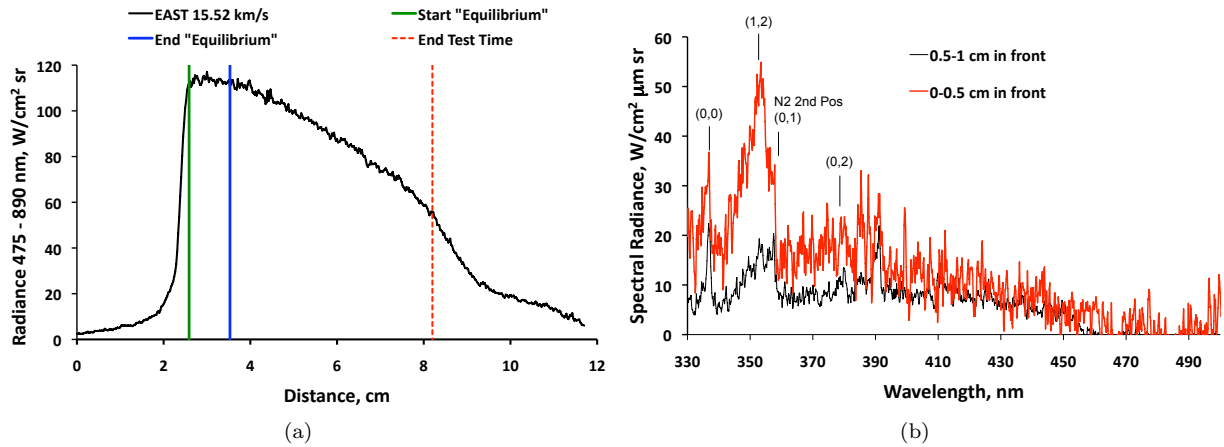

Figure 5. EAST Shot T52-15 at 15.52 km/s and 0.1 Torr showing (a) nominal equilibrium cross-section for the Vis/NIR spectral region and (b) spectral profiles ahead of the shock.

IV. Overall NEQAIR and HARA Maximum and Minimum Uncertainty Bounds

Due to the large number of shots performed in the EAST facility, there is an excellent basis for a statistical analysis of the data. In this way, the effect of shot-to-shot variation can be observed, and the level of scatter calculated. Furthermore, individual shots can be identified as "outliers" and radiance trends can be seen with respect to shock velocity. In order to develop an accurate assessment of how well NEQAIR and HARA simulate measured data, it is not necessary to base this assessment on individual shots, but rather by evaluating the simulations against sets of data.[13] However, due to the relatively small number of shots available at 0.2 Torr and at high speed (presently there are 5 shots above 11 km/s at 0.2 Torr), the results obtained at 0.1 Torr have been scaled to be consistent with the 0.2 Torr data. The 0.1 Torr shots have
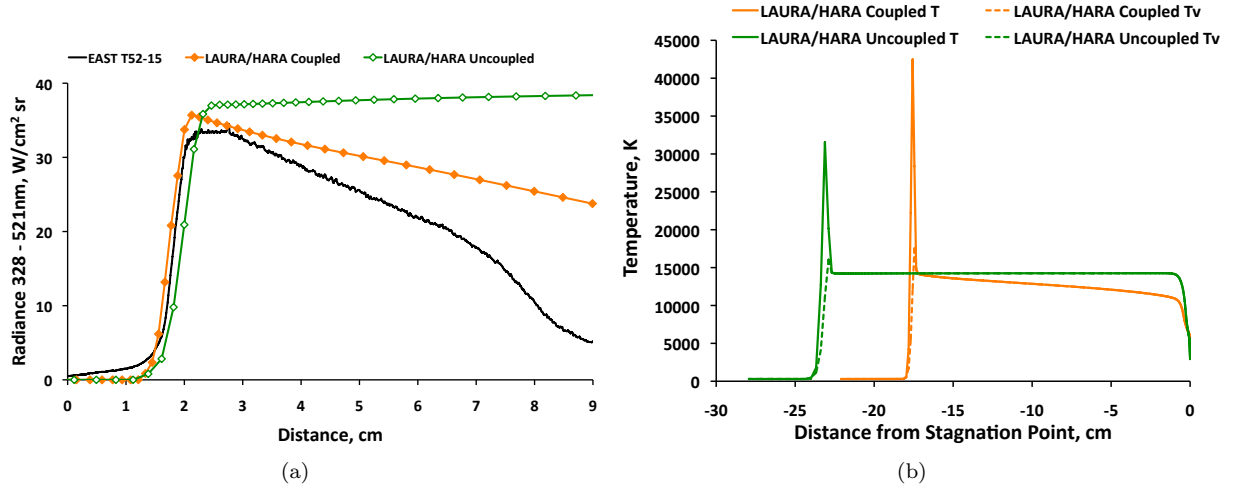
Figure 6. Comparison of EAST and LAURA/HARA for coupled and uncoupled cases for (a) radiance in the UV/Vis spectral range and (b) temperature profiles at 15.52 km/s and 0.1 Torr.

been scaled because, overall, there is still a greater number of shots at 0.2 Torr. The scaling factor has been calculated by performing a NEQAIR calculation at pressures of 0.1 and 0.2 Torr for the given shock speed of the experiment, and calculating the ratio of the integrated radiances for the relevant spectral range. This process is represented in Equation 1:

$$I_{EXP_{scaled}} = I_{EXP_{0.1}} \times \frac{I_{NEQ_{0.2}}}{I_{NEQ_{0.1}}} \tag{1}$$

where $I_{EXP_{scaled}}$ represents the scaled 0.1 Torr data, $I_{EXP_{0.1}}$ represents the original 0.1 Torr data, $I_{NEQ_{0.2}}$ represents the NEQAIR result calculated at 0.2 Torr and $I_{NEQ_{0.1}}$ represents the NEQAIR result calculated at 0.1 Torr. An example showing the 0.2 Torr along with the scaled 0.1 Torr data is shown in Fig. 7(a) for the 730 – 890 nm spectral region. It should be noted that the scaled 0.1 Torr data will have the same relative difference compared to the NEQAIR result at 0.2 Torr as the original 0.1 Torr data would when compared to NEQAIR results calculated at 0.1 Torr. However, by including the 0.1 Torr data, the trend of the EAST data can be extended in shock velocity, and due to the analysis being based on more data points, increased confidence is then obtained in the trend of the EAST results.

IV.A. Methodology

This section presents the methodology for calculating the upper and lower uncertainty bounds for NEQAIR and HARA's prediction of EAST. Firstly, each shot is analyzed to classify the quality of the equilibrium plateau reached behind the shock.[13] In the case of the higher speed shots, such as presented in Fig. 5(a), the equilibrium region is found in approximately the first 1 cm directly behind the shock. Only a small region of equilibrium test time is often observed in these shots before the effect of radiative cooling begins to become significant. Following this, each spectral region and feature of each shot is integrated and plotted as a function of velocity. A function is then fit to the integrated EAST data for the shots showing the best equilibrium characteristics. The coefficients for the fits have been calculated using the software *Igor* with 1 of 3 functional forms. These forms have been denoted as Modified Arrhenius (Eq. 2; abbreviated to Mod Arrh), Hill (Eq. 3) and Modified Hill (Eq. 4; abbreviated to Mod Hill). These functional forms are shown below:

$$I(v) = x_1 \times (v + x_4)^{x_2} \times e^{\frac{x_3}{v + x_4}} + m \times v + c \tag{2}$$

$$I(v) = x_1 + \frac{x_2 - x_1}{1 + (\frac{x_3}{v})^{x_4}} \tag{3}$$

$$I(v) = x_1 + \frac{x_2 - x_1}{1 + (\frac{x_3}{v})^{x_4}} + m \times v + c \tag{4}$$

The Hill equation was developed as a functional form for applications in biochemistry, with the form being similar to a sigmoidal function.[27] It has been noted that there is a strong connection between the Hill equation and the laws of equilibrium reactions,[28,29] as it has been used to fit experimental data from various physiochemical reactions, such as enzymatic reactions,[30] acetylcholine on muscular cells[31] and absorption of molecules on surfaces.[32] These examples, as indicated by Goutelle et al.,[27] suggest there are some arguments for a relative universality of equilibrium principles. Equations 2 and 4 also contain a linear component to the fit ($m \times v + c$). The linear component was added to improve the fits for some of the spectral ranges at shock speeds lower than approximately 9.5 km/s. Without the linear component, some fits showed a bias to over-predict the EAST result at these lower speeds. The fit chosen for each spectral region is determined by minimizing both the standard deviation and mean of the residuals (the residual being the difference of each EAST data point to the fit, normalized by the fit).

Figure 7(a) shows an example where the Hill functional form has been applied to the 0.2 Torr and scaled 0.1 Torr EAST data for the $730 - 89$ nm spectral range. The percentage deviation from each point to the fit is determined, and from this, the mean and standard deviation in the scatter of EAST is calculated, as seen in Fig. 7(b). Uncertainty in the shock speed is in this way contained within the standard deviation, provided that the error in shock speed follows a random distribution. A function is then calculated that is the relative difference of the computational results and the fit of the EAST data, normalized against the experimental value, to provide an error in terms of the relative uncertainty. This function is shown as the solid red curve in Fig. 7(c). Finally, the standard deviation in the scatter of the EAST data and the 95% confidence interval (CI) of the EAST mean is added and subtracted to this function, providing the upper and lower uncertainty bounds for each spectral region, refer to the solid black lines and dashed red lines in Fig. 7(c) respectively. The 95% confidence interval is calculated using t-distribution statistics due to the relatively small data-set sample size and being in close proximity to a normal distribution. The confidence intervals are evaluated through the following formula:

$$\bar{x}_n - t_{a,n-1} \times \frac{S_n}{\sqrt{n}} \leq \bar{I} \leq \bar{x}_n + t_{a,n-1} \times \frac{S_n}{\sqrt{n}} \tag{5}$$

where $\bar{x}_n$ is the sample mean, n is the number of samples, $t_{a,n-1}$ is the t score evaluated at $a\%$ confidence and $n-1$ degrees of freedom and S_n is the sample standard deviation

For the particular example of Fig. 7(c) the mean difference between NEQAIR and EAST for this region spans from 9 to -14% over the velocity range of 10 to 15.5 km/s. The figure also shows the 95% confidence interval in the mean EAST result being [7.4%, -4.8%] with one standard deviation in the scatter of the EAST results being 16.5%. It would be overly conservative to use this as error bounds over the entire trajectory, when in fact the error can be described as a velocity-dependent bias, plus the 95% confidence interval to provide an assessment of the experimental uncertainty.

IV.B. Results

Once the bounds for each spectral region and feature have been determined as a function of velocity, the influence of these uncertainties on the overall uncertainty can be evaluated. This is achieved by weighting each spectral range uncertainty by the amount of radiance emitted in each specific wavelength region. The weighting is evaluated by using the EAST fits as the baseline. For each spectral range, the percentage of the emitted radiation in that range compared to the overall radiation emitted is deemed to be the weighting factor. The weighting factors can then be used as a multiplier for each wavelength range, and then summed over all the spectral regions investigated to obtain the overall uncertainty. This process is represented by equation 6, where U_{tot} is the total uncertainty, n is the number of spectral ranges investigated, I_j is the intensity for the jth spectral region, I_{tot} is the total intensity defined in equation 7 and U_j is the uncertainty for the jth spectral region.[13]

$$U_{tot} = \sum_{j=1}^{n} \frac{I_j}{I_{tot}} \times U_j \tag{6}$$

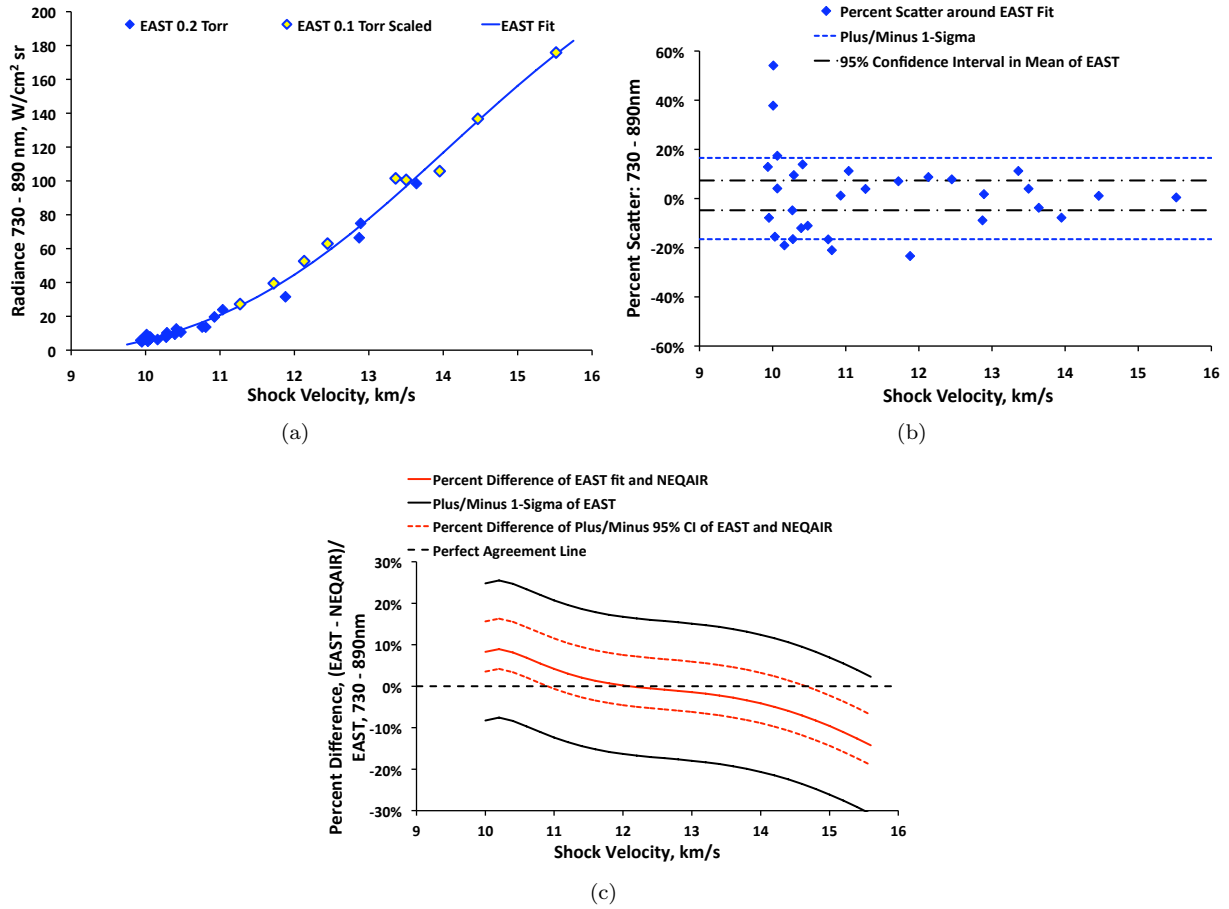$$I_{tot} = \sum_{j=1}^{n} I_j \tag{7}$$

Figure 7. Method for obtaining upper and lower uncertainty for each spectral feature. (a) Fitting EAST with a function, (b) Calculating standard deviation from scatter of EAST results around the fit, (c) Uncertainty for NEQAIR's prediction of the 730 - 890 nm spectral region of EAST.

American Institute of Aeronautics and Astronautics

Information regarding the individual spectral regions fits are provided in Tables 2 and 3. Table 2 shows the coefficients for each fit of each region analyzed. These fits can be used for comparisons of trends found in the EAST data with other experiments or simulations. There are some gaps in the wavelength regions analyzed due to these regions either containing contamination lines (usually H-alpha or carbon), have no significant spectral features or having not yet been measured at high speed. The standard deviation of the scatter around the fit and the 95% confidence interval in the mean of the EAST data at 13 km/s is also presented in Table 3 to give an idea of the significance of any discrepancies between future comparisons of simulations with EAST. Finally, the sum of residuals from the fit is provided to give an indication of any bias in the fit (this value is also the sample mean used in the calculation of the confidence intervals). Figures showing the comparison of NEQAIR, HARA and EAST with 0.2 Torr and scaled 0.1 Torr EAST data covering from the VUV to IR spectral regions are shown in Appendix A. For each wavelength range the comparison is shown on both a log and linear scale. The log scale has been used to highlight the overall trend of the comparison and any discrepancies at the lower speeds. The linear scale has been used to highlight the significance of the uncertainty and the 95% confidence intervals, while also showing any discrepancies at the higher speeds. An example of three such plots is shown in Fig. 8. The reason these three plots have been used as an example is to show the biggest discrepancy between the codes and EAST (Fig. 8(a)), and the biggest discrepancy between the two codes (Figs. 8(b) and 8(c)).

Figure 8(a) shows that at speeds around 10 km/s both codes are in close agreement with EAST, however, between 10.5 and 14.5 km/s, there is a substantial over-prediction of the 174 nm nitrogen line. Not only is the magnitude not in good agreement, but the trend between the codes and EAST is different. It was hypothesized that boundary layer absorption not accounted for in the simulations could be responsible for the disagreements. Therefore, the potential for boundary layer absorption causing a decrease in the measured radiation was investigated by approximating the boundary layer as a thin constant property layer, through which the radiation from the core flow must pass. The pressure of this thin layer was assumed equal to the core flow and in chemical equilibrium at a range of temperatures from 1000 to 8000 K, while the thickness of this layer was varied from 0.5 to 2 cm. For all cases, the only noticeable absorption occurred below 140 nm and the boundary layer did not contribute any noticable emission. The influence of the boundary layer on the present measurements is therefore limited to the decrease in the path length of the core flow, which is equal to twice the boundary layer thickness. For optically thin regions of the spectrum, this path length decrease will result in a proportional decrease in the measured intensity. Without a full CFD solution of the EAST facility available, it is presently assumed that the boundary layer thickness is negligible.

Uncertainty in Stark broadening parameters has previously been shown to influence the intensity of VUV radiance (approximately a $10 - 15\%$ change in intensity when the Stark width is increased or decreased by a factor of 2 at 10.98 km/s and 0.15 Torr).[2] However, if it is assumed that this relationship of Stark broadening and radiative intensity is constant with shock speed, the 15% increase would not be sufficient to provide perfect agreement between the simulations and experiment.

Uncertainty in the flow temperature of EAST could plausibly provide a reason for the discrepancy as the 174 nm nitrogen line is strongly absorbed ($> 99\%$ of the total emission is absorbed), and therefore the intensity is strongly dependent on temperature. According to a calculation performed with NEQAIR, for the condition at 13.64 km/s and 0.2 Torr, a decrease of 2% and 5% from the nominal equilibrium temperature results in a reduction of the radiance by 15% and 35% respectively. This level of reduction in radiance is similar in magnitude to what would be needed to provide good agreement between the simulations and experiment. If the temperature is indeed less than equilibrium (as shown in the coupled LAURA/HARA solution presented in Fig. 6(b)), it could be an indication of the presence of radiative cooling taking effect in the nominated equilibrium region of the flow.

Figures 8(b) and 8(c) shows a comparison between the 2 codes and EAST for a spectral region dominated by background continuum, and is therefore an example of the biggest discrepancy between NEQAIR and HARA. As previously mentioned, HARA models the contribution to the continuum from electron attachment which is not implemented in NEQAIR and uses a curve fit for the bound-free where as NEQAIR implements the full TOPBase database. The magnitude in the differences between NEQAIR and HARA for the various mechanisms providing continuum radiation is shown in Fig. 9. Figure 9 shows that the most significant contributor to the background continuum is that resulting from bound-free nitrogen. It is also clear from the figure, that by implementing the full cross sections from TOPbase, the nitrogen bound-free continuum is significantly higher in VUV/UV spectral range (from approximately 200 - 250 nm). Furthermore, Figs. 9(a) and 9(b) show that the continuum resulting from N^- is comparable in magnitude to that of the nitrogen

bound-free at 10 km/s. However, at 15.5 km/s, the N$^-$ is relatively negligible, as seen in Figs. 9(c) and 9(d). The TOPBase lines implemented in HARA can also clearly be observed in Figs. 3(b) and 4(b) and appear to be significantly stronger than those present in the EAST data. The superposition of these TOPBase lines (and corresponding line wings) may also provide an elevated level of background continuum. If the TOPBase lines were to be removed from the HARA simulation, the integrated intensity in the UV/Vis from 330 to 480 nm at 13.64 km/s and 0.2 Torr would decrease from approximately 35 W/cm^2 sr to 32 W/cm^2 sr and therefore be in closer agreement to EAST. These differences in implementation are the source of the discrepancies seen between the NEQAIR and HARA results presented in Fig. 8(b) and 8(c). Figure 8(b) shows that NEQAIR shows very good agreement with EAST while HARA under-predicts this background continuum dominated spectral region. The spectral range shown in Fig. 8(c) is a little more complicated as atomic emission is also present. The figure shows that from approximately 10 to 12 km/s, both NEQAIR and HARA are in good agreement with the EAST data. However, from 12 to 15.5 km/s, the HARA result begins to over predict EAST.
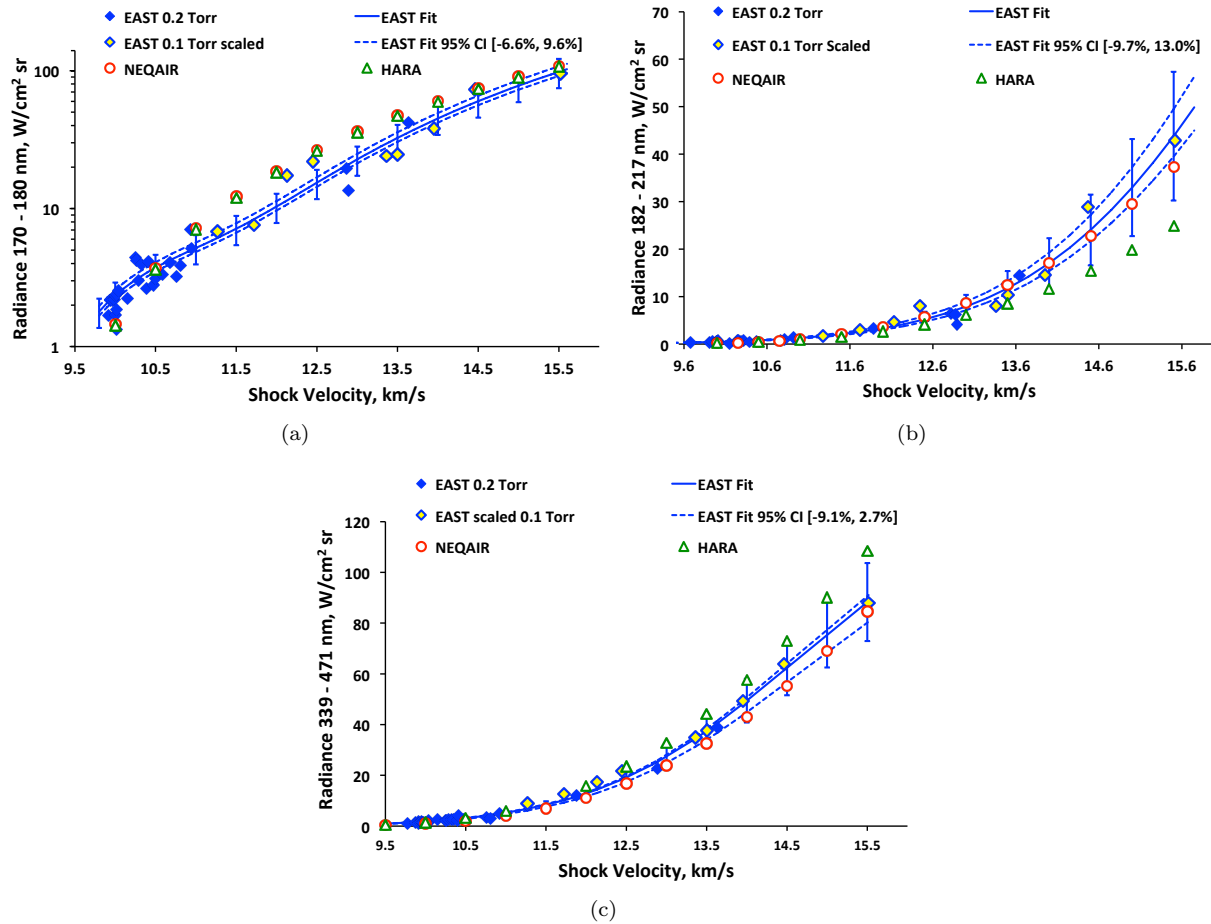

(a)

(b)

(c)

Figure 8. Comparison of EAST, NEQAIR and HARA for the (a) 170 − 180 nm spectral region, (b) 182 − 217 nm spectral region and (c) 339 − 471 nm spectral region versus shock velocity.

Figure 10 shows a plot of the EAST fits evaluated at shock speeds of 11, 12, 13, 14 and 15 km/s with comparisons to the results obtained from NEQAIR and HARA. It should be noted that the significance of the VUV is reduced in this figure compared to what has previously been reported,[13] and this is due to the limited wavelength range the data obtained in EAST during the high speed test campaign (Test 52). The previous analysis extended in the VUV down to 129 nm,[13] while this analysis only shows data to 170 nm. As has been previously mentioned, it was concluded by Brandis et al.[13] that EAST shows good equilibrium characteristics for shock speeds from 10 − 11.5 km/s, and consequently the experimental results were shown to be in good agreement with both NEQAIR and HARA. From the results presented in Fig. 10 this good agreement can be seen to continue up to shocks speeds of 15.5 km/s. This would indicate that
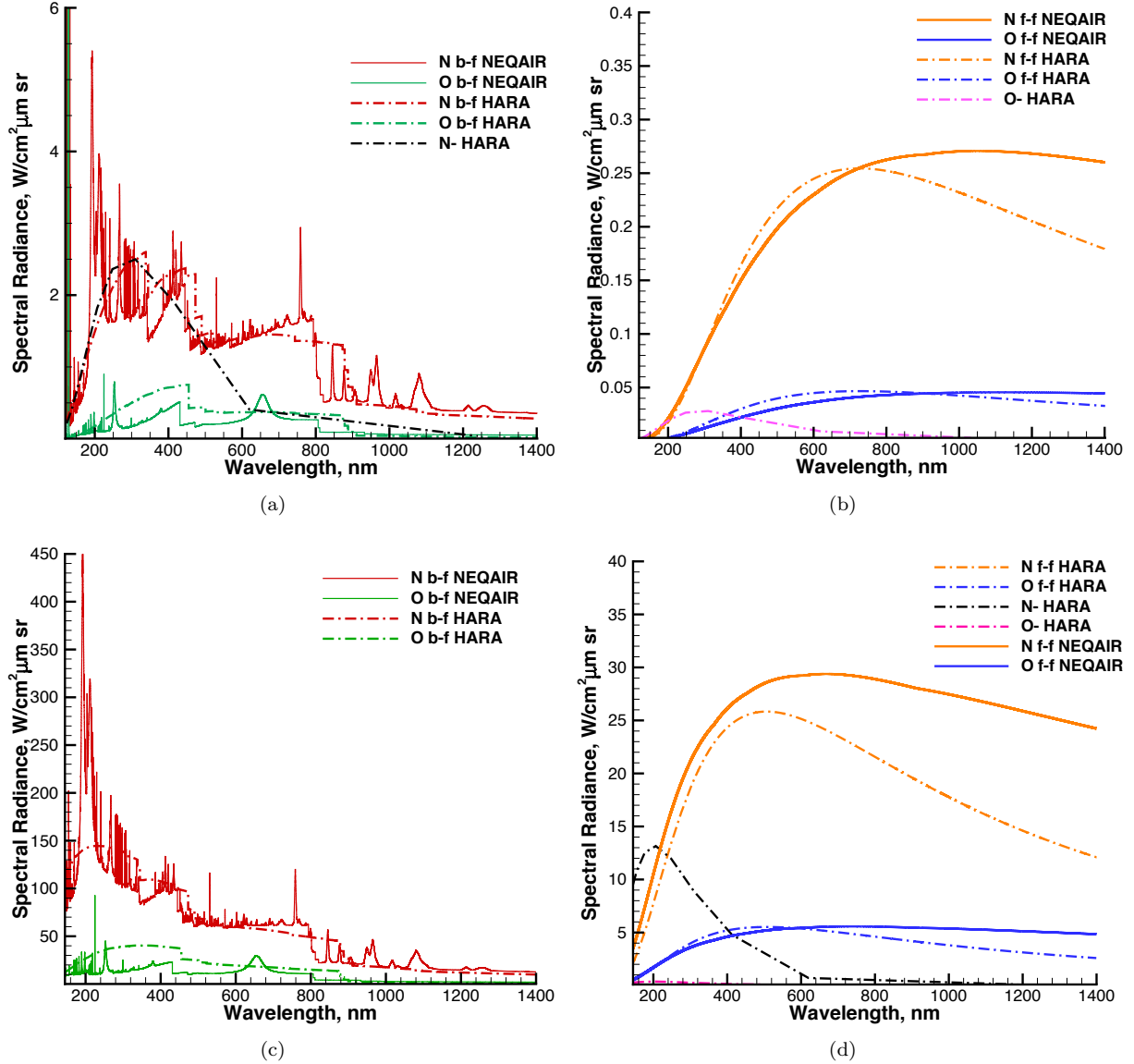
American Institute of Aeronautics and Astronautics

Figure 9. Comparison of continuum radiation mechanisms implemented in NEQAIR and HARA at 10 km/s and 0.2 Torr for (a) Bound-Free (b) Free-Free and at 15.5 km/s and 0.1 Torr for (c) Bound-Free (d) Free-Free.

American Institute of Aeronautics and Astronautics

the trend of electron number density measurements[12] in EAST reaching equilibrium for shock speeds faster than approximately 10.2 km/s continues to higher speeds. The good agreement is especially highlighted for both NEQAIR and HARA in the Vis/NIR, where both codes are on average within 4% of the EAST result and in the IR where both codes are within 13%. The agreement is found to be the worst for the VUV where NEQAIR and HARA are on average within 45% (peaking at 80%). As has been reported earlier, the biggest difference between the two codes is in the UV/Vis, where HARA is on average within 7% of the EAST result, while NEQAIR is on average within 12% of EAST.

Table 2. Spectral regions investigated, including fit coefficients and range of fit validity at 0.2 Torr

Spectral Range, nm	Fit Type	EAST Coefficients $I(v) = f(x_1, x_2, x_3, x_4, m, c)$ $[W/(cm^2 sr)]$	Range of Fit Validity, $v[km/s]$
170 - 180	Mod Arrh	15.171, 1.6535, -6.9304, -9.7865, 2.7706, -25.359	9.8 - 15.6
182 - 217	Hill	0.0015479, 172.23, 17.073, 11.133, –, –	9.6 - 15.6
339 - 471	Hill	-0.18631, 145.98, 14.895, 10.743, –, –	9 - 15.6
507 - 556	Mod Hill	5.8109, 80.798, 15.552, 7.6954, -1.3805, 6.0259	10 - 15.6
567 - 648	Mod Hill	2.8949, 120.39, 15.87, 7.9317, -0.94205, 4.1582	10 - 15.6
663 - 704	Mod Hill	8.4922, 90.739, 15.514, 7.0805, -2.0134, 8.6139	10 - 15.6
730 - 890	Hill	-8.8728, 283.27, 14.51, 7.8827, –, –	10 - 15.6
890 - 1185	Mod Hill	117.56, 1120.2, 15.411, 5.6747, -31.942, 127.14	9.6 - 15.6
1185 - 1334	Hill	-1.4719, 116.99, 14.334, 10.41, –, –	10.4 - 15.6
1334 - 1388	Hill	-0.47451, 30.121, 14.386, 9.9129, –, –	10.4 - 15.6

Table 3. Spectral regions investigated, including standard deviation, percentage of total emitted radiation at 13 km/s, 95% confidence interval and sum of fit residuals.

Spectral Range, nm	1-Sigma of EAST Scatter	Percent Radiation of EAST at 13.0 km/s	95 % Confidence Intervals	Sum of Residuals
170 - 180	26.8%	7.3%	[-6.6%, 9.6%]	1.5%
182 - 217	31.0%	2.5%	[-9.7%, 13.0%]	1.7%
339 - 471	17.4%	8.7%	[-9.1%, 2.7%]	-3.3%
507 - 556	17.0%	2.9%	[-8.4%, 6.6%]	-0.9%
567 - 648	22.8%	4.8%	[-10.5%, 9.8%]	-0.3%
663 - 704	16.0%	3.0%	[-7.0%, 5.6%]	-0.7%
730 - 890	16.5%	24.8%	[-4.8%, 7.4%]	1.3%
890 - 1185	13.5%	33.9%	[-5.9%, 4.8%]	-0.6%
1185 - 1334	15.6%	9.6%	[-7.3%, 6.6%]	-0.3%
1334 - 1388	14.9%	2.5%	[-6.8%, 6.4%]	-1.5%

Results of the overall summation of uncertainty are shown in Fig. 11. The level of agreement is reported in terms of the 95% confidence of the mean, rather than the standard deviation in the level of scatter of the EAST result (as was previously reported by Brandis et al.[13]). Figure 11 shows the percent disagreement of the models with respect to the mean EAST result and the corresponding 95% confidence intervals. The figure shows that from approximately 9.8 km/s to 11 km/s, both codes are under-predicting the EAST data. Some of this disagreement, as suggested by the electron number density data presented by Cruden,[12] could be due to chemical nonequilibrium flow effects in EAST. Between 9.6 km/s and 10.2 km/s, the electron number density was significantly higher than equilibrium. Consequently, by using the electron number density calculated at equilibrium, the radiation would in turn be under-predicted (as shown in Fig. 11). At present, the best hypothesis for the higher than equilibrium electron number density measurement relates to the deceleration of the shock due to viscous effects. This attenuation of the shock may cause the observed data to reflect the elevated temperature and density created at the higher shock speeds upstream of the test section.[10,33,34] From 10.2 to 11 km/s the electron number density measurements began approaching equilibrium. This is
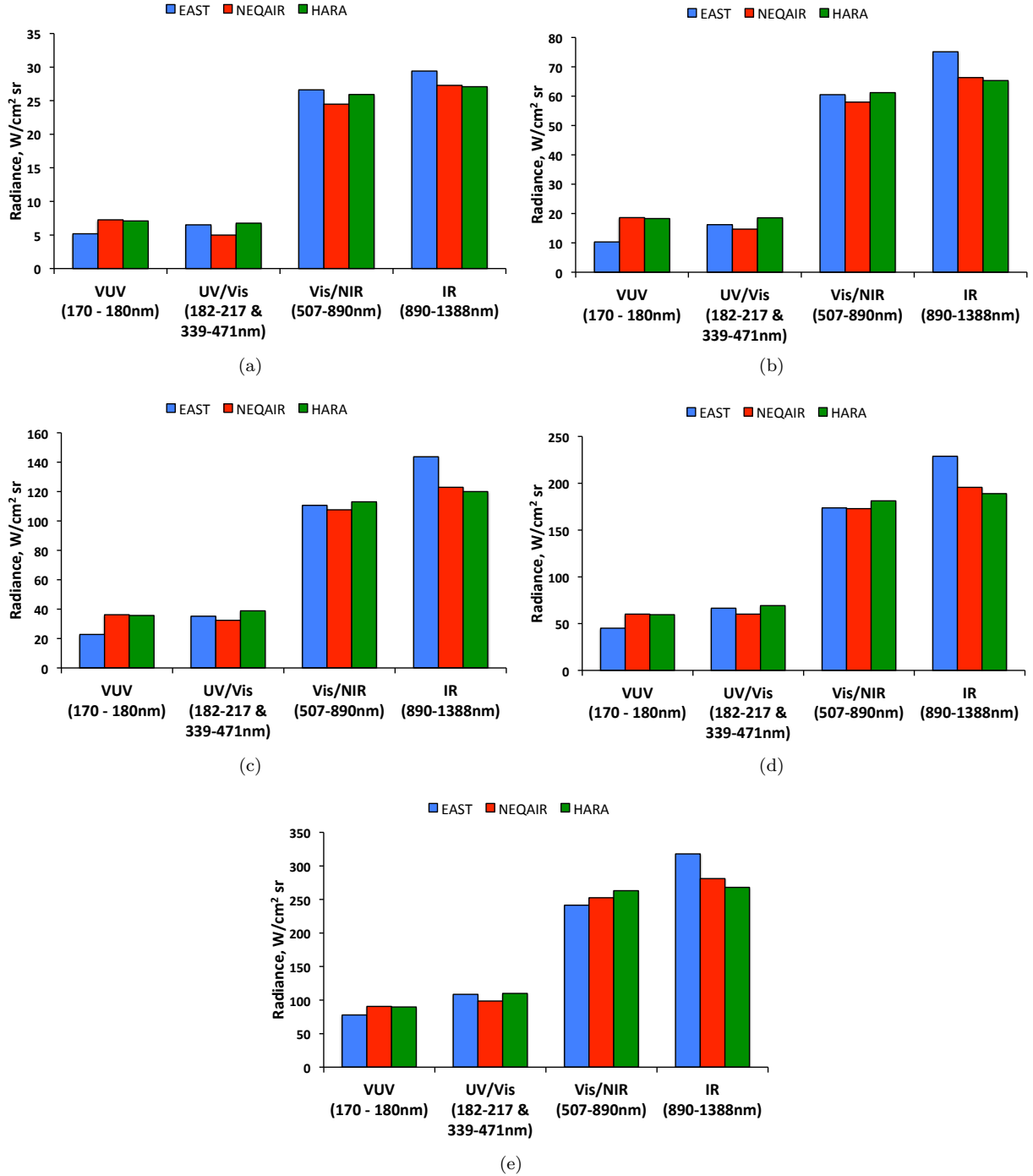
Figure 10. Contributions of the VUV (170 - 180 nm), UV/Vis (182 - 217 & 339 - 471 nm), Vis/NIR (507 - 890 nm) and IR (890 - 1388 nm) spectral regions at (a) 11 km/s, (b) 12 km/s (c) 13 km/s, (d) 14 km/s and (e) 15 km/s.

American Institute of Aeronautics and Astronautics

reflected in Fig. 11 where from 9.8 to 10.8 km/s both codes are showing an improving level of agreement to the EAST result. Then, from 10.8 to 15.5 km/s the agreement between both codes is excellent. This excellent level of agreement indicates that EAST remains in equilibrium at high speed. Furthermore, these results show that for conditions when the EAST facility is showing good equilibrium characteristics, the equilibrium calculations performed with NEQAIR and HARA predict the measured radiance very well. Both codes are either close to, or within, the 95% confidence interval of the experimental data. By including radiative attachment and the atomic lines from TOPbase, closer agreement is obtained with the experimental results at low speed. However, this may be fortuitous agreement due to the increase in electron number density observed in EAST compared to equilibrium. While it is clear that at least some of the TOPbase lines absent from NIST are present in experiment, the accuracy of these coefficients still needs to be assessed. It is less clear whether the radiative attachment mechanism is accurately modeled, as the available cross-sections for this process were derived over 40 years ago before the potential energy curves of N^- were well understood.[35] The influence of these uncertainties in HARA is discussed in Johnston et al.[9]

Finally, the maximum and minimum difference between the ± 95% confidence interval of either simulation and EAST is used to provide an updated parametric uncertainty for high speed Earth entry. This results in a parametric uncertainty bound for air radiation of [9.0%, -6.3%] on average. The level of agreement with the EAST data as presented in this paper has significantly improved compared to previously reported values.[36] The improved agreement is due to the updates implemented in the latest release of NEQAIR, in particular using TOPBase for continuum radiation. This improved level of agreement is highlighted in Fig. 8(b), a spectral region where the previous version of NEQAIR showed a substantial under prediction.[36]

The parametric uncertainty quoted by Johnston et al.[9] accounted for the uncertainty in stagnation point radiative heating resulting from the uncertainty in parameters related to both air and ablation products at shock speeds ranging from 11 to 15 km/s. The analysis covered uncertainty in atomic and molecular band oscillator strengths, atomic line stark broadening, atomic photoionization, Opacity Project lines, negative ion photo-detachment, ionization potential lowering and photo-ionization edge shifts. As the present work does not simulate any effect due to ablation, the total updated parametric uncertainty is now presented to be the bounding average percent differences between the NEQAIR, HARA and EAST results combined with the uncertainty related to ablation products as quoted by Johnston et al.[9] Structural uncertainties in the baseline simulations due to turbulence modeling, precursor absorption, grid convergence, and radiative transport uncertainties was determined by Johnston et al.[9] to be [34%, -24%]. A summary of the previous and updated parametric, structural and total uncertainty at a range of shock speeds from 11 to 15 km/s is shown in Table 4. The table shows that on average there is a 15% to 30% reduction in the parametric uncertainty compared to the previous values reported by Johnston et al.[9]

Table 4. Summary of parametric, structural and total uncertainties for radiative heating at 11, 12, 13, 14 and 15 km/s.

	11 km/s	12 km/s	13 km/s	14 km/s	15 km/s
Previous Parametric[9] Uncertainty	[41.1%, -36.9%]	[43.8%, -34.2%]	[45.0%, -32.4%]	[46.3%, -30.8%]	[47.3%, -28.3%]
Updated Parametric Uncertainty	[12.2%, -12.7%]	[17.4%, -13.7%]	[19.3%, -14.3%]	[22.0%, -14.4%]	[24.2%, -13.6%]
Structural Uncertainty[9]	[34.0%, -24.0%]	[34.0%, -24.0%]	[34.0%, -24.0%]	[34.0%, -24.0%]	[34.0%, -24.0%]
Updated Total Uncertainty	[46.2%, -36.7%]	[51.4%, -37.7%]	[53.3%, -38.3%]	[56.0%, -38.4%]	[58.2%, -37.6%]

V. Conclusion

The recent high speed testing in EAST has provided the first spectrally and spatially resolved radiance measurements for shock speeds up to 15.5 km/s. The results presented in this paper provide a validation and comparison of simulation tools and EAST data for a high shock speed Earth entry regime. The integrated radiance for four spectral regions has been analyzed and compared between NEQAIR, HARA and the nominal
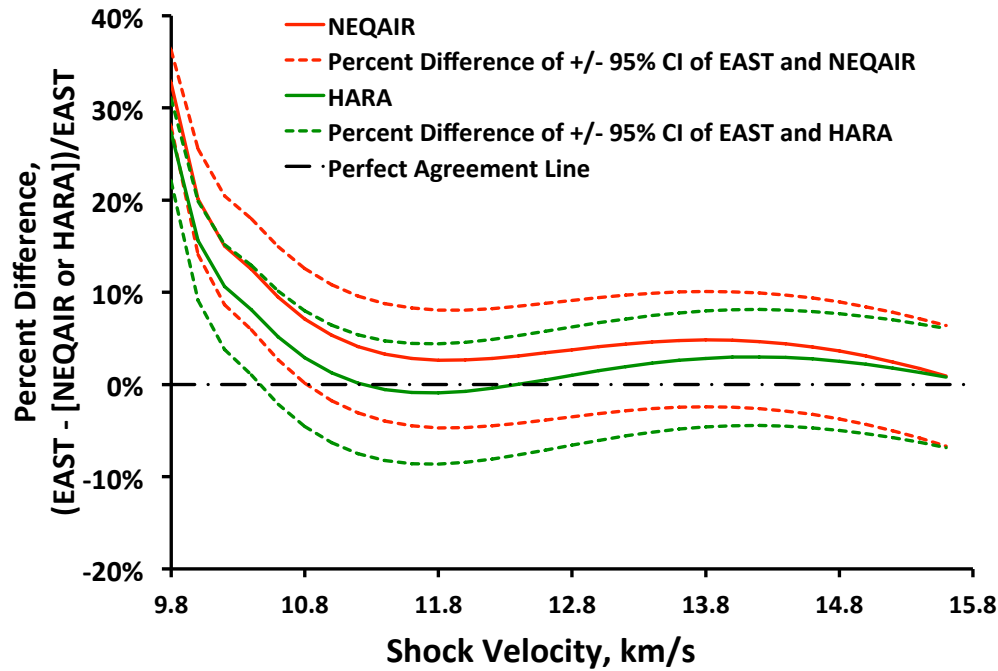
Figure 11. Overall percent disagreement of NEQAIR and HARA's prediction with respect to EAST from 170 - 1388 nm including 95% confidence intervals.

equilibrium results obtained from the EAST data. The results have shown very good agreement between NEQAIR and HARA for the UV through IR spectral regions. HARA predicts a larger radiance in the UV/Vis spectral region due to the inclusion of the radiative attachment mechanisms, which offers some improved agreement to EAST at lower velocities (9 - 12 km/s) but an apparent over-prediction at higher velocities (12 - 15.5 km/s). Discrepancies in the VUV for NEQAIR and HARA have been observed with some evidence suggesting this could be linked to uncertainties in the equilibrium temperature of the shocked EAST test gas. The spectral comparisons of NEQAIR, HARA and EAST in the Vis/NIR spectral region show excellent agreement in terms of both the line intensities and the appearance of the level of the background continuum. The overall percentage disagreement of the models with respect to EAST for 0.2 Torr at 10 km/s is within 20% and from 11 to 15.5 km/s is on average within 2.5%. The overall 95% confidence interval in the mean of the EAST result is on average [5.8%, -7.2%] and the overall standard deviation in the scatter of EAST is ± 17%. An updated bound for the parametric uncertainty for high speed Earth entry has been determined to be [9.0%, -6.3%]. This is a significant reduction in the radiative heating uncertainty for high speed entry as it was previously calculated to be [32%, -21%][9] at 15 km/s prior to the EAST tests presented in this paper. The high speed EAST measurements also provide a unique data set for the validation of radiative cooling mechanisms implemented in a coupled CFD/radiation solver (such as LAURA and HARA) and analyzing precursor radiation. The analysis showed that a significant amount of radiative cooling is observed, but the amount is under-predicted when compared to experiment.

Overall, even though good agreement has been observed between NEQAIR, HARA and EAST, some discrepancies have been identified. The most significant of these being: 1) the under-prediction of the IR spectral range, 2) the discrepancies observed in the VUV and 3) the trend to a worsening level of agreement of the codes compared to experiment at slower shock speeds. Therefore, the focus of future testing should be to re-examine EAST experiments at slower shock speeds (possibly employing a mixture of argon and helium in the driver gas to improve the equilibrium characteristics of the flow), conduct high speed experiments in the deep VUV while also taking measurements that would allow the calculation of electron number density.

References

[1]Johnston, C., "A Comparison of the East Shock-Tube Data with a New Air Radiation Model," Reno, Nevada, January 2008, AIAA 2008-1245.

[2]Bose, D., McCorkle, E., Thompson, C., Bogdanoff, D., Prabhu, D., Allen, G., and Grinstead, J., "Analysis and Model Validation of Shock Layer Radiation in Air," *AIAA*, Reno, Nevada, January 2008, AIAA 2008-1246.

[3]Panesi, M., Magin, T., Bourdon, A., Bultel, A., and Chazot, O., "Analysis of the Fire II Flight Experiment by means of a Collisional Radiative Model," *Journal of Thermophysics and Heat Transfer*, Vol. 23, No. 2, 2009, pp. 236–248.

[4]Panesi, M., Magin, T., Bourdon, A., Bultel, A., and Chazot, O., "Study of electronically excited state populations of atoms and molecules predicted by means of a collisional-radiative model for the Fire II flight experiment," *Journal of Thermophysics and Heat Transfer*, Vol. 25, 2011, pp. 361–374.

[5]Cruden, B., Martinez, R., Grinstead, J., and Olejniczak, J., "Simultaneous Vacuum-Ultraviolet Through Near-IR Absolute Radiation Measurement with Spatiotemporal Resolution in An Electric Arc Shock Tube," *41st AIAA Thermophysics Conference*, San Antonio, Texas, 2009, AIAA-2009-4240.

[6]Whiting, E., Park, C., Yen, L., Arnold, J., and Paterson, J., "NEQAIR96, Nonequilibrium and Equilibrium Radiative Transport and Spectra Program: User's Manual," Technical Report NASA RP-1389, Ames Research Center, Moffett Field, Moffett Field, 1996.

[7]Johnston, C., Hollis, B., and Sutton, K., "Spectrum Modeling for Air Shock-Layer Radiation at Lunar-Return Conditions," *Journal of Spacecraft and Rockets*, Vol. 45, No. 5, 2008, pp. 865–878.

[8]Johnston, C. O., Hollis, B., and Sutton, K., "Non-Boltzmann Modeling for Air Shock Layers at Lunar Return Conditions," *Journal of Spacecraft and Rockets*, Sep.-Oct. 2008.

[9]Johnston, C., Mazaheri, A., Gnoffo, P., Kleb, B., Sutton, K., Prabhu, D., Brandis, A., and Bose, D., "Assessment of Radiative Heating Uncertainty for Hyperbolic Earth Entry," *42nd AIAA Thermophysics Conference*, Honolulu, 2011.

[10]Grinstead, J. H., Olejniczak, J., Wilder, M. C., Bogdanoff, D. W., Allen, G. A., and Lilliar, R., "Shock-heated Air Radiation Measurements at Lunar Return Conditions," *46th AIAA Aerospace Sciences Meeting and Exhibit*, 7-10 January 2008, Reno, Nevada 2008, AIAA-2008-1244.

[11]Bogdanoff, D. W., "Shock tube experiments for Earth and Mars entry conditions," *Non-equilibrium gas dynamics, from physical models to hypersonic flights*, Vol. Von Karman Institute Lecture Series, 2008.

[12]Cruden, B., "Electron Density Measurement in Re-entry Shocks for Lunar Return," *Journal of Thermophysics and Heat Transfer*, Vol. 26, 2012, pp. 222.

[13]Brandis, A., Johnston, C., Cruden, B., Prabhu, D., and Bose, D., "Uncertainty Analysis and Validation of Radiation Measurements for Earth Re-Entry," *Journal of Thermophysics and Heat Transfer*, Vol. 29, No. 2, 2015, pp. 209–221.

[14]Kramida, A., Ralchenko, Y., Reader, J., and Team, N. A., "NIST Atomic Spectra Database, Version 5.0.0," physics.nist.gov/asd/, July 2012, last accessed July, 2012.

[15]Cunto, W., Mendoza, C., Ochsenbein, F., and Zeippen, C., "TOPbase at the CDS," *Astronomy and Astrophysics*, Vol. 275, Aug. 1993, pp. L5–L8, see also http://cdsweb.u-strasbg.fr/topbase/topbase.html.

[16]Peach, G., "Continuous Absorption Coefficients for Non-hydrogenic Atoms," *Memoirs of the Royal Astronomical Society*, Vol. 73, 1970, pp. 1–123.

[17]Tashkun, S. and Perevalov, V., "CDSD-4000: High-Resolution, High-Temperature Carbon Dioxide Spectroscopic Databank," *Journal of Quantitative Spectroscopy and Radiative Transfer*, Vol. 112, No. 9, 2011, pp. 1403–1410.

[18]Cruden, B. and Brandis, A., "Updates to the NEQAIR Radiation Solver," St. Andrews, Scotland, November 2014.

[19]Ralchenko, Y., "NIST Atomic Spectra Database, Version 3.1.0," physics.nist.gov/PhysRefData/ASD/, July 2006, last accessed September 3rd, 2007.

[20]The Opacity Project Team, *The Opacity Project*, Vol. 1, Bristol and Philadelphia: Institute of Physics Publishing, 1995.

[21]Johnston, C. O., Hollis, B. R., and Sutton, K., "Radiative Heating Methodology for the Huygens Probe," *Journal of Spacecraft and Rockets*, Vol. 44, No. 5, 2007, pp. 993–1002.

[22]McBride, B. and Gordon, S., "Computer Program for Calculation of Complex Chemical Equilibrium Compositions and Applications I. Analysis," NASA RP-1311, NASA Glenn, October 1994.

[23]Program Development Company, Tech. rep., 300 Hamilton Avenue,Suite 409, White Plains, NY 10601.

[24]Wright, M., White, T., and Mangini, N., "Data-Parallel Line Relaxation (DPLR) Code User Manual Acadia-Version 4.01.1," NASA/TM-2009-215388, NASA Ames Research Center, October 2009.

[25]Park, C., "Review of chemical-kinetic problems for future NASA missions, I. Earth entries," *Journal of Thermophysics and Heat Transfer*, Vol. 7, 1993, pp. 385–398.

[26]Bose, D., McCorkle, E., Bogdanoff, D. W., and Allen Jr., G., "Comparisons of air radiation model with shock tube measurements." *47th AIAA Aerospace Sciences Meeting*, Orlando, Florida, 2009, AIAA-2009-1030.

[27]Goutelle, S., Maurin, M., Rougier, F., Barbaut, X. Bourguignon, L., Ducher, M., and Maire, P., "The Hill equation: a review of its capabilities in pharmacological modelling," *Societe Francaise de Pharmacologie et de Therapeatique Fundamental and Clinical Pharmocology*, Vol. 22, 2008, pp. 633–648.

[28]Clark, A., "The mode of action of drugs on cells," *Edward Arnold and Co, London*, 1933.

[29]McLean, F., "Application of the law of chemical equilibrium (law of mass action) to biological problems," *Physiology Review*, Vol. 18, 1933, pp. 495–523.

[30]Michaelis, L. and Menten, M., "Die kinetic der Invertinwirkung." *Biochem. Z*, Vol. 49, 1913, pp. 333–369.

[31]Clark, A., "The reaction between acetyl choline and muscle cells," *The Journal of Physiology*, Vol. 61, 1926, pp. 530–546.

[32]Langmuir, I., "The constitution and fundamental properties of solids and liquids. Part 1 Solids." *Journal of the American Chemical Society*, Vol. 38, 1916, pp. 2221–2295.

[33]Light, G., "Test Gas Properties Behind a Decelerating Shock Wave in a Shock Tube," *The Physics of Fluids*, Vol. 16, No. 5, 1973, pp. 624–628.

[34]Brandis, A., Cruden, B., Prabhu, D., Bose, D., McGilvray, M., and Morgan, R., "Analysis of Air Radiation Measurements Obtained in the EAST and X2 Shocktube Facilities," *10th AIAA/ASME Joint Thermophysics and Heat Transfer Conference*, Chicago, Illinois, 2010, AIAA 2010-4510.

[35]Asinovsky, E., Kirillin, A., and Kobzev, G., "Investigation of Continuum Radiation of Nitrogen Plasma," *Journal of Quantitative Spectroscopy and Radiative Transfer*, Vol. 10, No. 3, 1970, pp. 143–164.

[36]Brandis, A., Johnston, C., Cruden, B., Prabhu, D., and Bose, D., "Validation of High Speed Earth Atmospheric Entry Radiative Heating from 9.5 to 15.5 km/s," *43rd AIAA Thermophysics Conference*, New Orleans, Louisiana, 2012, AIAA-2012-2865.

Appendix A

Appendix A presents comparisons of NEQAIR, HARA and EAST for all the spectral regions analyzed in this paper. For each spectral range the 95% confidence interval of EAST is shown with the 1 sigma standard deviation in the level of scatter in the EAST result being indicated by the error bars. The comparisons are also shown on both a log and linear scale. The log scale has been used to highlight the overall trend of the comparison and any discrepancies at the lower speeds. The linear scale has been used to highlight the significance of the uncertainty and confidence intervals, while also showing any discrepancies at the higher speeds. Figure 12 shows results for the VUV where discrepancies can be observed between the codes and the experimental result. Figures 13 and 14 show the results in the UV/Vis, where the biggest discrepancies between the two codes can be observed as these regions are dominated by the background continuum. Figures 15 to 18 show the results for the Vis/NIR where excellent agreement between both codes and EAST can be observed. Figures 19 to 21 show the results for the IR, where both codes are in good agreement with each other, but under-predict the results shown by EAST.
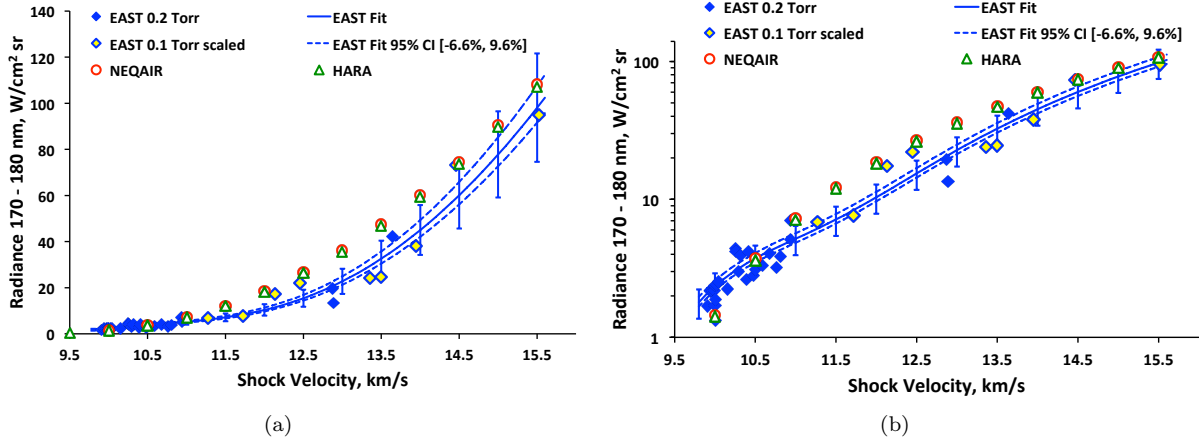
Figure 12. Comparison of EAST, NEQAIR and HARA for the 170 − 180 nm spectral region versus shock velocity on a (a) linear scale (b) log scale.
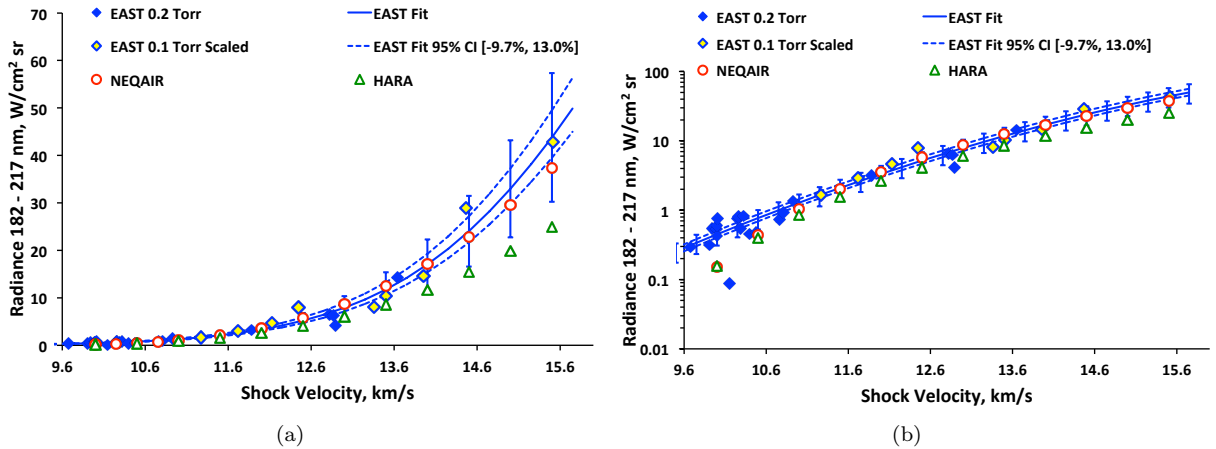
Figure 13. Comparison of EAST, NEQAIR and HARA for the 182 − 217 nm spectral region versus shock velocity on a (a) linear scale (b) log scale.
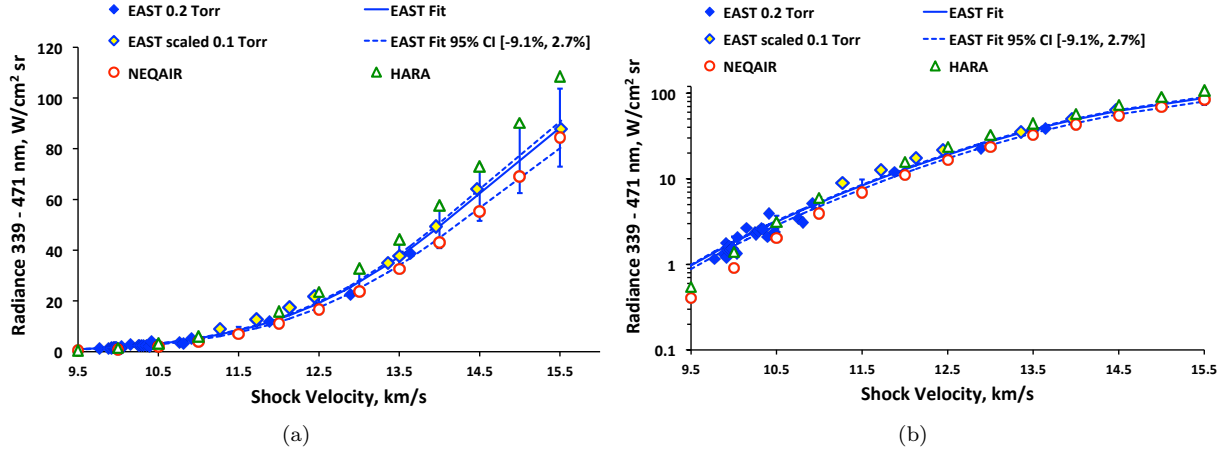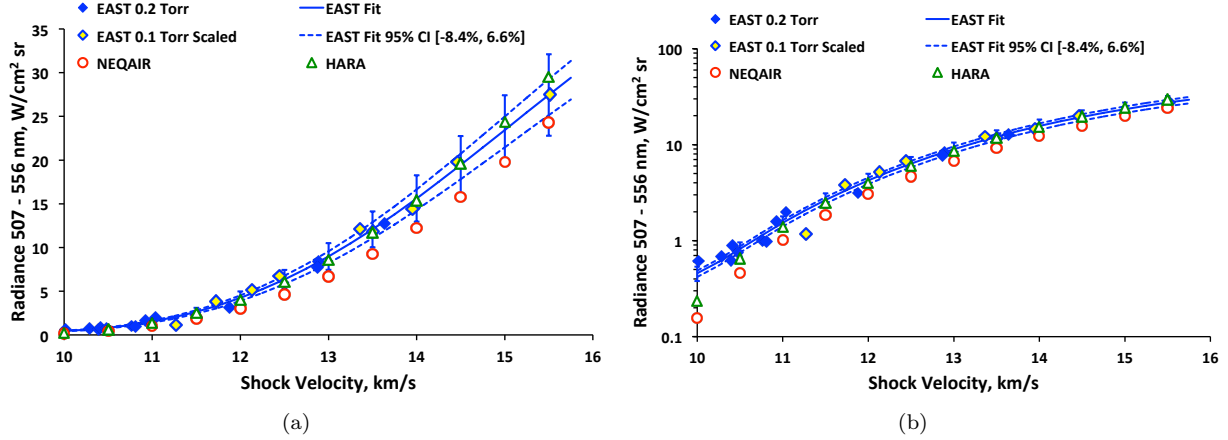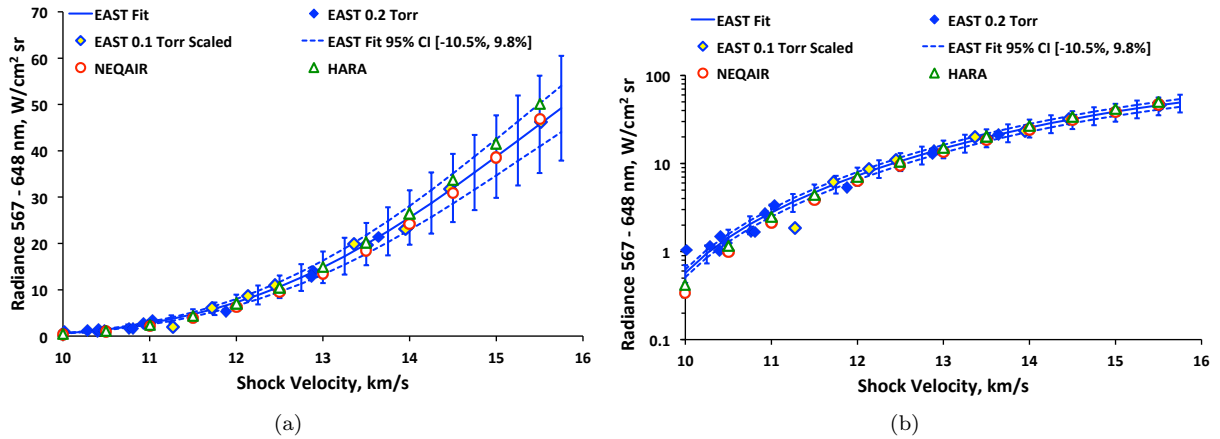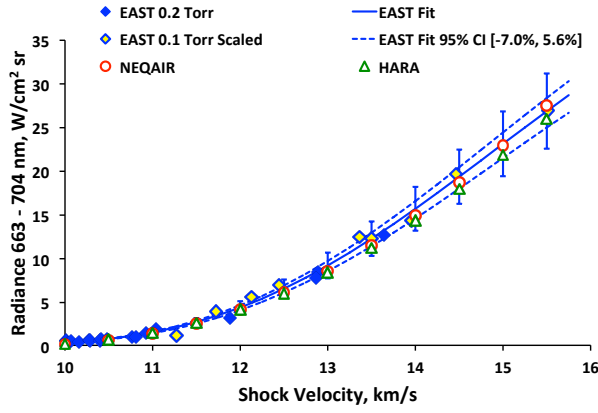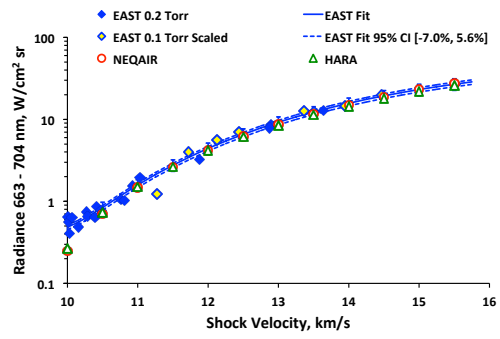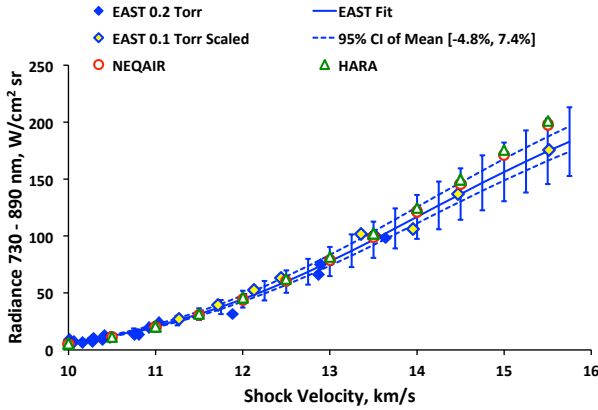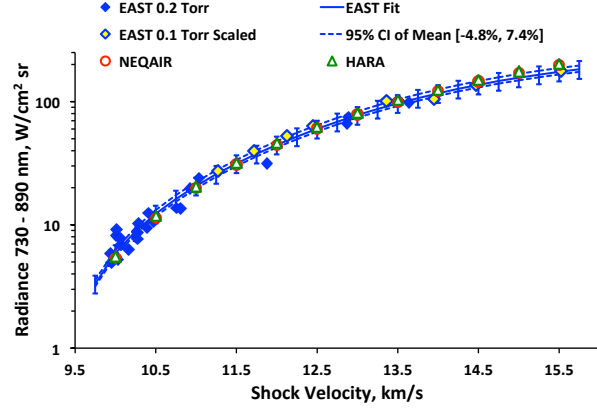
American Institute of Aeronautics and Astronautics

Figure 14. Comparison of EAST, NEQAIR and HARA for the $339 - 471$ nm spectral region versus shock velocity on a (a) linear scale (b) log scale.

Figure 15. Comparison of EAST, NEQAIR and HARA for the $507 - 556$ nm spectral region versus shock velocity on a (a) linear scale (b) log scale.

Figure 16. Comparison of EAST, NEQAIR and HARA for the $567 - 648$ nm spectral region versus shock velocity on a (a) linear scale (b) log scale.

American Institute of Aeronautics and Astronautics

Figure 17. Comparison of EAST, NEQAIR and HARA for the 663 − 704 nm spectral region versus shock velocity on a (a) linear scale (b) log scale.
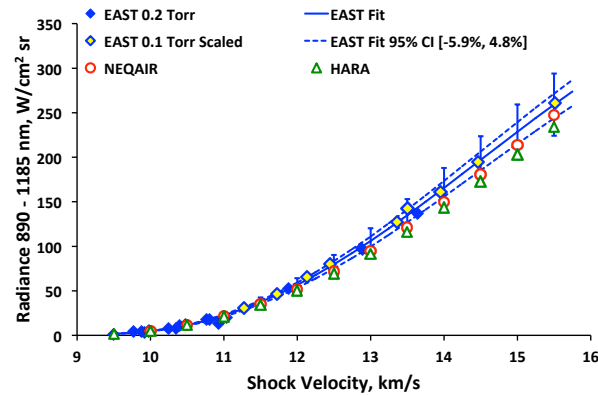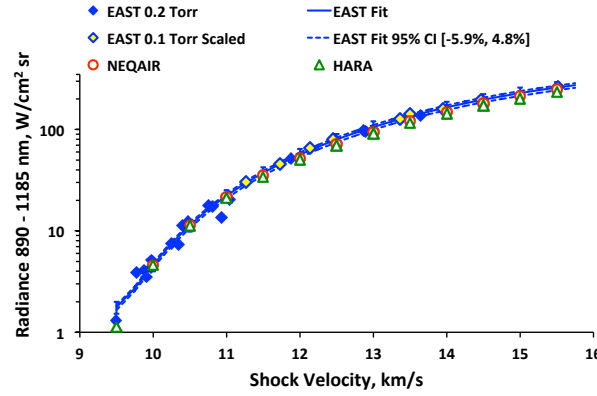

Figure 18. Comparison of EAST, NEQAIR and HARA for the 730 − 890 nm spectral region versus shock velocity on a (a) linear scale (b) log scale.

Figure 19. Comparison of EAST, NEQAIR and HARA for the 890 − 1185 nm spectral region versus shock velocity on a (a) linear scale (b) log scale.
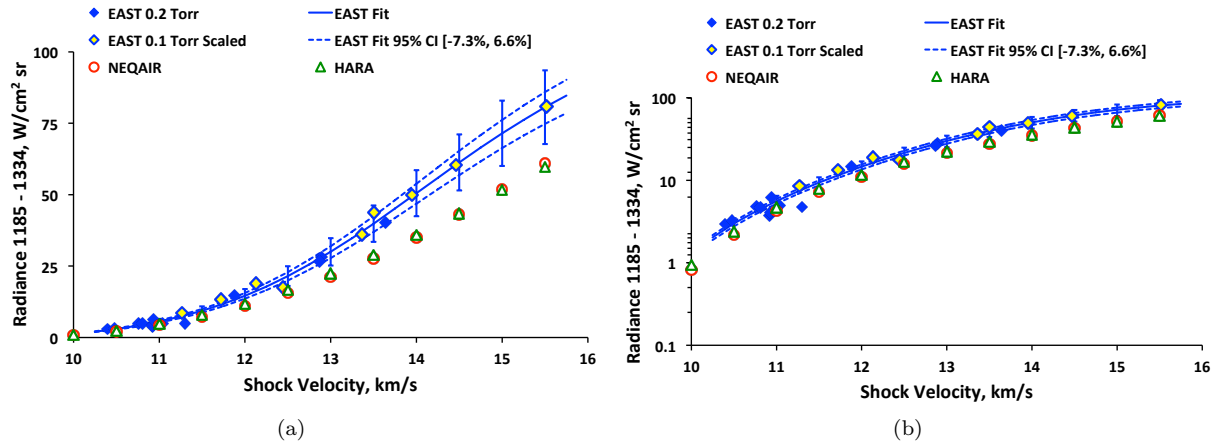
American Institute of Aeronautics and Astronautics

Figure 20. Comparison of EAST, NEQAIR and HARA for the $1185 - 1334$ nm spectral region versus shock velocity on a (a) linear scale (b) log scale.
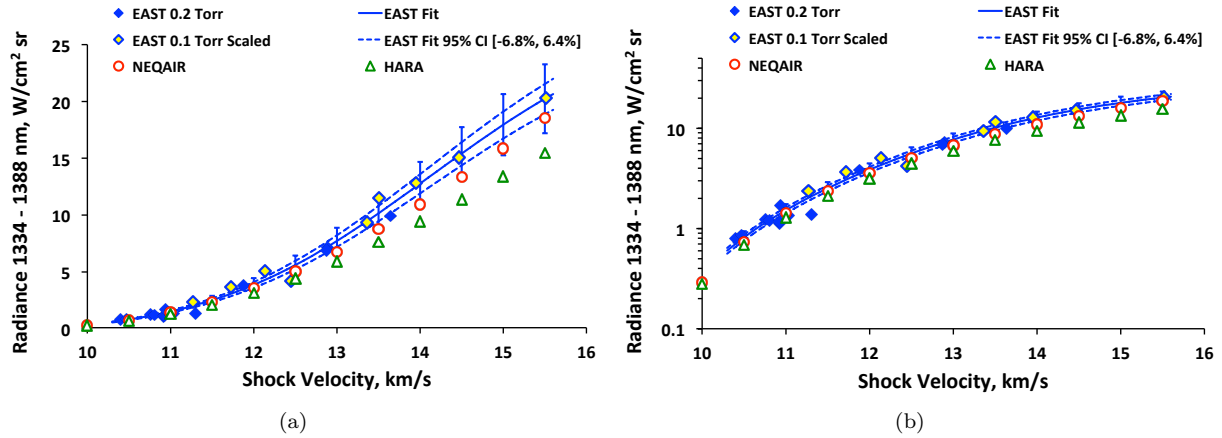

Figure 21. Comparison of EAST, NEQAIR and HARA for the $1334 - 1388$ nm spectral region versus shock velocity on a (a) linear scale (b) log scale.

American Institute of Aeronautics and Astronautics